THE JOURNAL OF PHYSICAL CHEMISTRY B

ARTICLE

pubs.acs.org/JPCB

The Structure of Aqueous Solutions of a Hydrophilic Ionic Liquid: The Full Concentration Range of 1-Ethyl-3-methylimidazolium Ethylsulfate and Water

Carlos E. S. Bernardes,*[,†,‡] Manuel E. Minas da Piedade,[‡] and José N. Canongia Lopes*[,†,§]

[†]Centro de Química Estrutural, Instituto Superior Técnico, UTL, 1049-001 Lisboa, Portugal

[‡]Departamento de Química e Bioquímica, Faculdade de Ciências, Universidade de Lisboa, 1649-016 Lisboa, Portugal

[§]Instituto de Tecnologia Química e Biológica, www.itqb.unl.pt, UNL, Av. República Ap. 127, 2780-901 Oeiras, Portugal

ABSTRACT: Several structural features of aqueous solutions of the ionic liquid 1-ethyl-3-methylimidazolium ethylsulfate were analyzed in the entire concentration range using molecular dynamics simulation results. Different analysis tools developed in-house were applied to describe the size and connectivity of different water and ion aggregates as a function of the solution concentration. Four concentration ranges—$x_{H_2O} < 0.5$, $0.5 < x_{H_2O} < 0.8$, $0.8 < x_{H_2O} < 0.95$, and $x_{H_2O} > 0.95$—with four distinct structural regimes—isolated water molecules, chain-like water aggregates, bicontinuous system, and isolated ions or small ion clusters — were identified and discussed, including two different percolation limits: that of water in the ionic liquid network (around $x_{H_2O} = 0.8$) and that of the ionic liquid in water (around $x_{H_2O} = 0.95$).

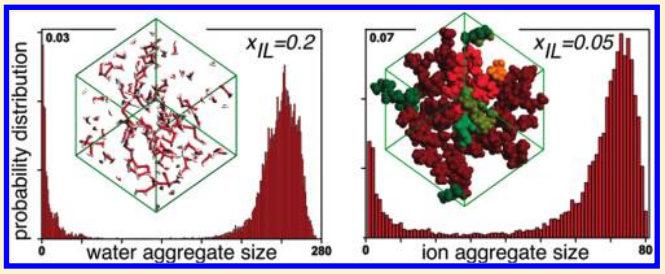

INTRODUCTION

Pure and applied research on ionic liquids has been gathering momentum since the late 1990s.[1−4] The key to this rising interest has been their unique physicochemical properties, such as very low vapor pressures, high conductivities, wide electrochemical windows, and large liquid ranges, limited by rather low melting point temperatures (generally below 100 °C) and high decomposition temperatures (above 200 °C in many cases). These features and the vast number of possible combinations of cationic and anionic components have, for example, fostered many efforts for the use of ionic liquids as task-specific solvents.

Several properties of ionic liquids (e.g., their density, viscosity, polarity, or conductivity) can be drastically changed by the presence of small amounts of other substances, and this may lead to significant modifications in, for example, the rate and selectivity of chemical reactions carried out in their midst.[3,5,6] Water is one of the most common types of impurities found in ionic liquids—even when not completely miscible with water, ionic liquids tend to be strongly hygroscopic. On the other hand, aqueous solutions of ionic liquids *per se* have became the subject of a variety of potential applications,[7−10] which motivated a significant number of fundamental studies of theoretical and experimental nature.[11−22]

Some of these works[12,14,23] have focused on aqueous solutions of imidazolium-based ionic liquids. They indicate that at low water concentrations the water molecules are isolated from each other or tend to exist in small independent clusters dispersed in a continuous polar network formed by the ionic liquid ions. As the water concentration rises, a continuous water network starts to build up and a nanosegregated bicontinuous system emerges. Finally, for water-richer compositions, the ionic liquid polar network starts to break apart, generating ion clusters dispersed in a continuous water phase.

We recently investigated the energetics of aqueous solutions of 1-ethyl-3-methylimidazolium ethylsulfate (Figure 1, $[C_2mim][EtSO_4]$) in the medium-to-high range of water molar fraction ($0.25 < x_{H_2O} < 0.9996$).[24] Flow and solution calorimetry experiments revealed the existence of a minimum in the enthalpy of solution curve at $x_{H_2O} = 0.99$, that could also be approximately captured by the results of molecular dynamics (MD) simulations ($x_{H_2O} = 0.94$). The interpretation of this minimum at a molecular level was carried out on the basis of MD simulations and energy partition schemes developed to separate the energy contributions from the IL−IL, H_2O-H_2O, and IL−H_2O interactions. It was concluded that the minimum essentially results from two opposing effects: (i) the fact that the differences between the IL−IL and H_2O-H_2O interaction energies in the solution and in the pure liquids are both positive and increase with the dilution of the IL and (ii) the simultaneously more negative character of the IL−H_2O contribution.

These trends should also reflect the structural modifications occurring in solution as the dilution proceeds. In this work, those structural changes are analyzed in light of further MD studies.

Received: November 29, 2010
Published: February 15, 2011

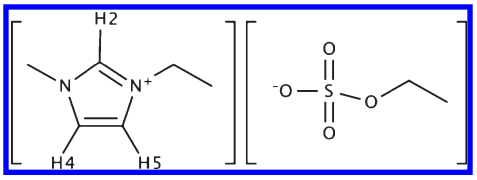

Figure 1. Molecular structure of 1-ethyl-3-methylimidazolium ethylsulfate, $[C_2mim][EtSO_4]$. The labeling scheme of the ring hydrogen atoms is that used in the text.

Table 1. Summary of the Simulation Box Composition Used in the Calculation of Different $[C_2mim][EtSO_4]$ Aqueous Solutions[a]

x_{H_2O}	N_{IL}	N_{H_2O}	x_{H_2O}	N_{IL}	N_{H_2O}
0.000	90	0	0.950	40	760
0.500	80	80	0.970	30	970
0.800	70	280	0.990	30	2970
0.900	60	540	0.996	12	2952
0.920	45	518	1.000	0	2000

[a] x_{H_2O} is the water molar fraction, and N_{IL} and N_{H_2O} are the number of ionic liquid pairs and water molecules in each simulation box.

METHODS

Molecular Dynamics (MD) Simulations. All aqueous solutions were simulated using the molecular dynamics package DL_POLY version 2.17.[24,25] Water and $[C_2mim][EtSO_4]$ were modeled by using the SPC model[26] and the force field developed by Canongia Lopes and co-workers,[27,28] respectively.

Simulation boxes containing solutions with x_{H_2O} = 0, 0.5, 0.8, 0.9, 0.92, 0.95, 0.97, 0.99, 0.996, and 1 were set by randomly placing the amounts of water molecules and ionic liquid ions given in Table 1 in a sufficiently large cubic grid (low density) to ensure an initial configuration with well separated molecules. These were then allowed to dynamically evolve under isothermal−isobaric ensemble (*N-p-T*) conditions at 298 K and 0.1 MPa. Typical runs consisted of an equilibration period of ∼1 ns followed by a production stage of 2 ns. During the production stage, configurations of the simulation box were recorded every 0.2 ps for subsequent structural analysis. A cutoff distance of 15 Å was used in all simulations. The Ewald summation technique with *k*-values set to 5 and α = 0.185 Å was applied beyond that distance.

Aggregate Analysis. The structures of the $[C_2mim][EtSO_4]$ aqueous solutions were analyzed by using an algorithm developed in the present work, based on some of the ideas put forward by Hanke and Lynden-Bell.[12] In order to study the clustering of water molecules in ionic liquids, these authors assumed that two water molecules belong to the same cluster if their O···O distance is smaller than 3.5 Å, which is the position of the first minimum in the O···O radial distribution function (RDF) given by MD simulations for the SPC/E model of pure water. This criterion allowed them to transform a list of intermolecular bonds into a series of water clusters. Here, a similar approach was adopted to analyze the evolution of the water aggregates and of the ionic liquid polar network as a function of the molar fraction of water, x_{H_2O}, in the solutions.

For the study of water aggregation (both in pure water and in the ionic liquid solutions), a connectivity criterion was first defined on the basis of the distance between the centers of mass

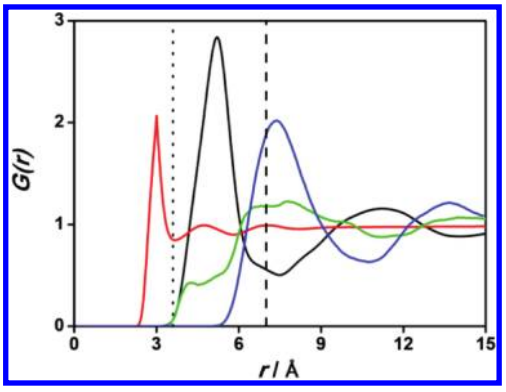

Figure 2. Radial distribution functions for the distances between the centers of mass of SPC water in pure water (red line), the centers of mass of the sulfate $-OSO_3$ group of the anions and the imidazolium ring of the cations in the pure ionic liquid (black line), the centers of mass of the sulfate $-OSO_3$ groups in the pure ionic liquid (blue line), and the centers of mass of the imidazolium ring of the cations (green line). The dotted and dashed lines mark the connectivity limits used in the aggregation analyses.

(wcm) of different water molecules. Two water molecules were considered to belong to the same aggregate if they lie in the first "coordination sphere" of each other. Following Hanke and Lynden-Bell's[12] rationale, the limit of this "coordination sphere" was set to 3.5 Å, which corresponds to the first minimum of the wcm−wcm radial distribution function (RDF) of pure SPC water obtained with the DL_POLY package (Figure 2, vertical dotted line). Not unexpectedly, because the water center of mass is almost coincident with the O atom, the selected cutoff distance matches that of Hanke and Lynden-Bell.[12] Once the connectivity criterion was defined, the following procedure was used: (i) The neighbor list of each water molecule was determined for each configuration recorded in the production stage of the simulation runs. (ii) The obtained neighbor lists were then used to establish the connectivity between all water molecules (i.e., water molecules separated by more than 3.5 Å can still belong to the same aggregate if they are linked through other water molecules that comply with the 3.5 Å criterion). Algorithms to cross-check the information in all neighbor lists were developed to complete this task. (iii) Finally, diverse statistical analyses concerning the distribution of aggregates as a function of x_{H_2O} were carried out (see below).

Unlike water aggregates composed of identical molecules, the ionic liquid clusters include two dissimilar ionic species of opposite charge. Thus, a modified version of the above-mentioned procedure had to be developed to address the ionic liquid polar network. Because oppositely charged ions attract one another, anions are more likely to be found near cations and vice versa. Indeed, it has been shown that ionic liquids preserve short-range charge ordering necessary to maintain local electroneutrality—cf. Figure 2 where the first peaks and throughs of the cation−anion RDF (black line) are opposite to the first throughs and peaks of the anion−anion and cation−cation RDFs (blue and green lines). Moreover, such ordering is determined by the parts of the ions where most of the charge (either positive or negative) is concentrated.[29−31] In the ionic liquid under discussion, the negative charge of the anions is mainly distributed among the oxygen atoms of the sulfate $-OSO_3$ group,[28] whereas the positive charge of the cation is located in the imidazolium ring.[27] Figure 2 depicts the RDF for the distances between the

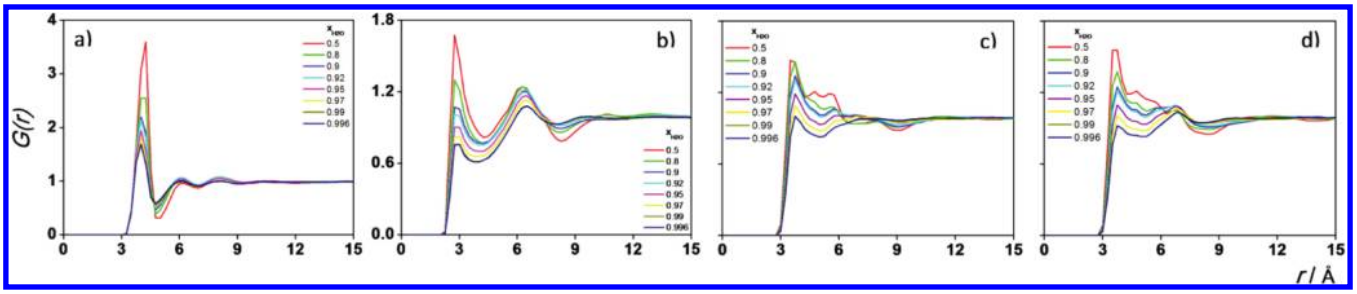

Figure 3. Radial distribution functions of the distances between the oxygen atom of water and (a) the sulfur atom of the ethylsulfate anion and (b) the H2, (c) H4, and (d) H5 atoms of the 1-ethyl-3-methylimidazolium cation (see the H labeling scheme in Figure 1), for different molar fractions of water, x_{H_2O}.

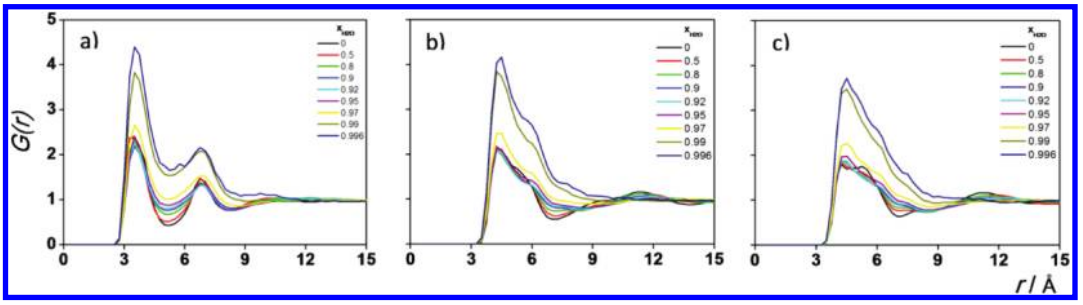

Figure 4. Radial distribution functions of the distances between the sulfur atom of the ethylsulfate anion and the (a) H2, (b) H4, and (c) H5 atoms of the 1-ethyl-3-methylimidazolium cation (see the H labeling scheme in Figure 1), for different molar fractions of water, x_{H_2O}.

centers of mass of those two groups and shows that the corresponding first coordination shell ends at approximately 7 Å (dashed line). This cutoff distance was therefore used to establish that a given cation and anion are connected and form a linkage in the ionic liquid polar network. Analogously to water, the neighbor lists of each cation or anion for every recorded configuration were generated and used to establish the connectivity within the polar network(s). The main departure from the case of water is that in the ionic liquid polar network the neighbor list of a given ion is exclusively composed of ions of opposite charge in order to model electrostatic cohesion. In other words, the connectivity within the network is such that any path through it must be a sequence of ions of alternating charge.

Several statistical functions were defined and evaluated to analyze the size and morphology of the water aggregates and ionic liquid networks: (i) The probability, $P(n)$, of finding a molecule or ion in an aggregate of size n (the number of molecules or ions in the aggregate) was calculated as

$$P(n) = \frac{n \cdot \sum_{j=1}^{C} A_n(j)}{C \cdot I} \quad (1)$$

where $A_n(j)$ is the number of aggregates of size n for a given configuration j, C is the total number of configurations acquired during the production stage, and I is the total number of ions (cations plus anions) or water molecules in the simulation box. (ii) The average number, N_i, of neighbors of each species i was evaluated as

$$N_i = \frac{\sum_{j=1}^{C} V_i(j)}{C \cdot I_i} \quad (2)$$

where $V_i(j)$ is the total number of neighbors of all water molecules or ions for a given configuration j and I_i is the number of molecules or ions of type i in the simulation box. Finally, (iii) the average number of neighbors of each species i in an aggregate of size n, $N_i(n)$, was calculated as

$$N_i(n) = \frac{\sum_{j=1}^{C} V_{i,n}(j)}{\sum_{j=1}^{C} I_i(j)} \quad (3)$$

where $V_{i,n}(j)$ is the total number of neighbors of species i in an aggregate of size n and $I_i(j)$ is the number of molecules or ions of the species i in the aggregates of size n.

RESULTS AND DISCUSSION

Local Structure. Radial distribution functions quantify the correlation between a specific atom and other similar or dissimilar atoms in its surroundings. They are one of the most convenient methods to extract structural information from simulation results and were used to characterize the structure of the $[C_2mim][EtSO_4]$ aqueous solutions, namely, (i) the local structure of water around the polar groups of the ionic liquid ions (Figure 3) and (ii) the local structure of the cationic and anionic moieties related to the formation of the ionic liquid polar network (Figure 4).

Figure 3 shows the RDFs for the distances between the oxygen atom of water (O_w) and the sulfur atom (S) of the ethylsulfate anion, or between O_w and the hydrogens H2, H4, and H5 in the $[C_2mim]^+$ cation (see Figure 1 for the H labeling scheme). These RDFs show that, for a given solution, the intensity of the first peak corresponding to the $O_w \cdots S$ distances (Figure 3a) is higher than those observed for the $O_w \cdots H2$, $O_w \cdots H4$, or $O_w \cdots H5$ counterparts (Figure 3b−d). This suggests stronger interactions between water and the ethylsulfate anion than

dx.doi.org/10.1021/jp1113202 |J. Phys. Chem. B 2011, 115, 2067–2074

between water and the imidazolium cation, in agreement with results for other ionic liquids.[13,15,21,29] Furthermore, the first peaks of the RDFs relative to the $O_w\cdots H2$ separations (Figure 3b) are slightly shifted to lower interatomic distances (by ~0.5 Å) relative to the first peaks of the RDFs corresponding to the $O_w\cdots H4/H5$ distances (Figure 3c and d). This last observation is related to the enhanced acidity of H2, and hence affinity for O_w, when compared to H4/H5.[15,18−20,29]

Figure 4 shows the RDFs for distances between selected atoms of the cation (H2, H4, and H5) and of the anion (S), revealing the types of interaction responsible for the formation of the polar network. Although for analogous solutions no significant differences in the intensities of the first solvation peaks are observed between the three types of interaction, the interaction between the S and H2 atoms occurs at distances ~1 Å smaller than those observed for the S and H4 or H5 atoms. Once again, this is a consequence of the acidic character of the H2 atom which leads to a preferential affinity for the polar group of the anion when compared to H4 and H5.[15,18−20,29]

It must be stressed at this point that the atoms selected to generate the different RDFs in Figures 3 and 4 are not necessarily those directly involved in a given interaction. Thus, for example, the water−anion interactions entailed by the hydrogen atoms of water and the oxygen atoms of the sulfate group were analyzed *via* RDFs involving the O_w and S atoms. The use of suitable proxy atoms is, however, justified in order to "clean" the RDFs from unnecessary extra peaks and shoulders originated by the presence of multiple, equivalent atoms at different distances.

The RDFs shown in Figures 3 and 4 exhibit systematical intensity changes with the concentration of the aqueous solutions. In the case of the water−ion interactions (Figure 3), the intensities decrease with the increasing dilution of the solutions, whereas, in the case of ion−ion interactions (Figure 4), the opposite trend is observed. However, this does not necessarily indicate that, as the solutions are diluted, the interactions between water and the ions become weaker or that those between ions become stronger. In fact, the observed intensity shifts are controlled by the concentration and heterogeneous distribution of each species in solution: in the case of ionic liquid-rich solutions, the water molecules tend to accumulate near the vicinity of selected parts of the polar network (the charged parts of the ions, especially the anion), giving rise to the highest first peaks of the RDFs in Figure 3. As the dilution advances, the water molecules start to accumulate more homogeneously (not only in the vicinity of the polar network as a whole but also around and inside increasingly larger water clusters), thus contributing to the observation of progressively less intense first peaks in Figure 3. In the case of the RDFs between the ionic liquid ions (Figure 4), the trend is the opposite for analogous reasons: the ion distribution is more homogeneous (less intense peaks) in ionic-liquid-rich solutions than in very diluted ionic liquid solutions, where the polar network is segregated and modified by progressively larger water aggregates that eventually form a second continuous microphase. It must be stressed that in this last case (Figure 4) the RDF intensity changes are only clear for $x_{H_2O} > 0.95$. As will be substantiated in the following sections, this threshold approximately marks the entrance in a concentration range where (i) the polar ionic liquid network starts to collapse and small ionic liquid aggregates or "icebergs" appear in the solution and (ii) the water aggregates begin to show structural features resembling those of pure water.

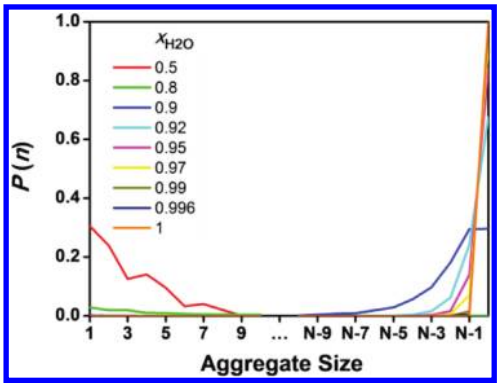

Figure 5. Size distribution of water aggregates as a function of solution composition. $P(n)$ is the probability of finding a water molecule in an aggregate of size n; x_{H_2O} is the water molar fraction. In the aggregate size axis, N represents the total number of water molecules in the simulation box (see Table 1 for details); for example, in a cluster of size N, all water molecules in the simulation box belong to the same aggregate.

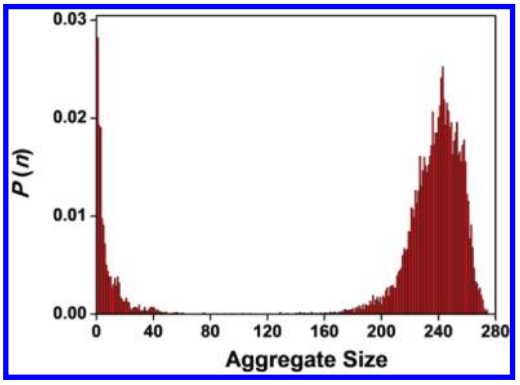

Figure 6. Size distribution of the water aggregates at $x_{H_2O} = 0.8$. $P(n)$ is the probability of finding a water molecule in an aggregate of size n.

Water Aggregation. Water clustering/aggregation was investigated by using the methodology described in the Methods section. Figure 5 shows the probability of finding a water molecule in an aggregate of size n, for different solution compositions. Three distinct tendencies can be observed in that figure: (i) for $x_{H_2O} \leq 0.5$, the molecules are isolated or belong to clusters with eight or less water molecules; (ii) for $0.5 < x_{H_2O} < 0.9$, a transition from small clusters to large aggregates occurs. This is clearly shown in Figure 6 where, for $x_{H_2O} = 0.8$, the water clusters span most of the possible size range and are therefore near the percolation limit of water in the ionic liquid solution; (iii) for $x_{H_2O} > 0.9$, almost all water molecules belong to a single large aggregate that spans the entire simulation box and effectively forms a second continuous phase, nanosegregated from the polar ionic liquid network (bicontinuous structure). Only a few isolated water molecules or small clusters detach from the continuous water network from time to time.

The observation that for $x_{H_2O} < 0.5$ the water molecules tend to be isolated, or in small aggregates, corroborates previous results obtained for other ionic liquid solutions.[12,18,21] These studies also revealed that, for low H_2O concentrations, the water molecules form linear chains. In fact, as shown in Figure 7 for solutions with $x_{H_2O} < 0.8$, the water molecules are surrounded by two or less other water molecules, suggesting the formation of linear chains. This is illustrated in Figure 8a and b, where the

linear nature of the water clusters surrounding the ionic liquid ions is clearly evidenced.

Figure 8c shows that water molecules in solutions with x_{H_2O} = 0.92 percolate the entire simulation box, forming a water network where each water molecule is connected on average to 3.5 other water molecules (Figure 7a). This branched sort of connectivity allows the H_2O molecules to shift from chain-like aggregates to a 3D web network that, together with the polar network of the ionic liquid, forms a bicontinuous structure for solutions in the concentration range $0.8 < x_{H_2O} < 0.95$.

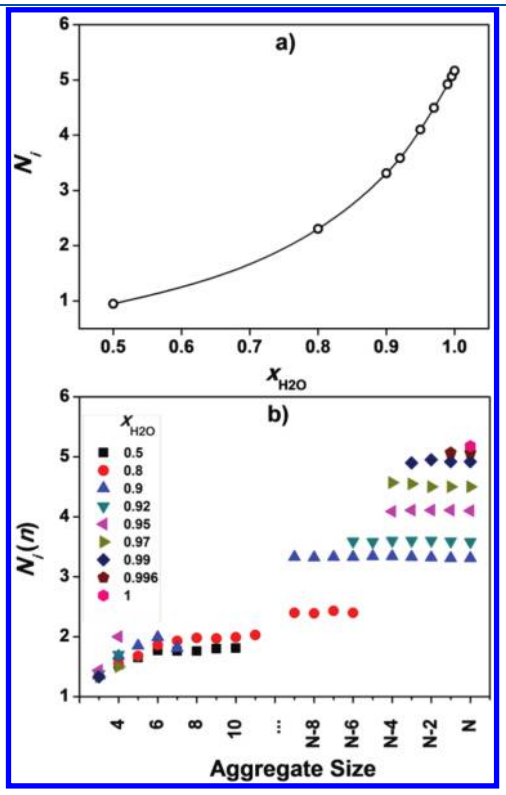

Figure 7. Number of water neighbors around water molecules. (a) Average number, N_i, of neighbors for all water molecules. (b) Average number of neighbors in clusters of size n, $N_i(n)$.

Interestingly, in the low limit of that range, at $x_{H_2O} \sim 0.8$, the water molecules contained in the continuous water network exhibit "coordination" numbers ($2 < N_{H_2O} < 3$), much smaller than those of pure water ($4 < N_{H_2O} < 5$). Figure 7a shows that only when $x_{H_2O} > 0.95$ does each H_2O molecule start to have more than four water neighbors in its first coordination shell. This means that a concentration of $x_{H_2O} > 0.95$ must be attained for the water aggregates to show structural features resembling those of pure water.

It is also important to remark that water aggregates with less than 10 molecules have an average number of neighbors of $N_i(n) \leq 2$ (lower left corner of Figure 7b), independently of the concentration of the solution and of the possible presence of other larger clusters. This is a clear indication that chain-like structures are the norm for these small clusters. Conversely, if we now consider aggregates that include almost all water molecules, we note that, for a given concentration, $N_i(n)$ is independent of the cluster size (upper right corner of Figure 7b). These results suggest that (i) the connectivity of the water network is dictated by the volume occupied by the ionic liquid polar network and (ii) the small aggregates detected for solutions with $x_{H_2O} > 0.8$ are probably originated by the detachment of terminal chains of molecules that have lower connectivity with the main aggregate. The threshold value $x_{H_2O} = 0.8$ is again present in Figure 7b, where at the center of the figure one can see the existence of very large aggregates with more than 200 molecules but with $N_i(n)$ values not much greater than 2, i.e., the formation at the percolation limit of a very thin, continuous chain-like structure around the polar network of the ionic liquid.

Ionic Liquid Aggregation. The size distribution of the ionic liquid aggregates is represented in Figure 9 as a function of the solution composition. As expected, the aggregates decrease in size with increasing water content. Figure 9 also shows that for $x_{H_2O} < 0.95$ the ions tend to belong to a single large aggregate (the polar network) which starts to fall apart only after this concentration threshold (which approximately corresponds to the ionic liquid percolating limit) is reached (Figure 10). It must be stressed that the existence of a continuous polar network in solutions with $x_{H_2O} < 0.95$ does not exclude the possibility of the existence of small ionic clusters that (temporarily) lose their connectivity to the polar network.

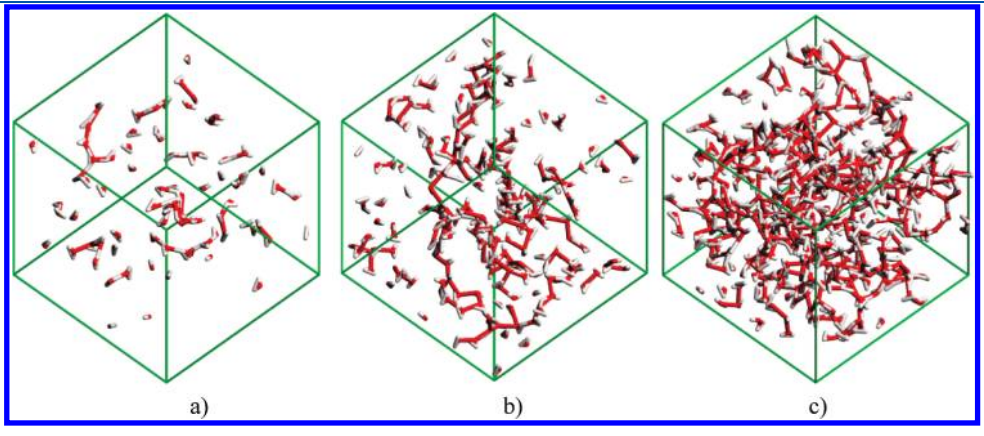

Figure 8. Snapshot images of the water clusters in simulation boxes with (a) $x_{H_2O} = 0.5$, (b) $x_{H_2O} = 0.8$, and (c) $x_{H_2O} = 0.92$. The pictures show that when small amounts of H_2O molecules are present they are either isolated or form chains around the polar network of the ionic liquid (not represented). When the water percolation limit is attained (between parts b and c), the water molecules form a continuous branched network surrounding the ionic liquid.

dx.doi.org/10.1021/jp1113202 |J. Phys. Chem. B 2011, 115, 2067–2074

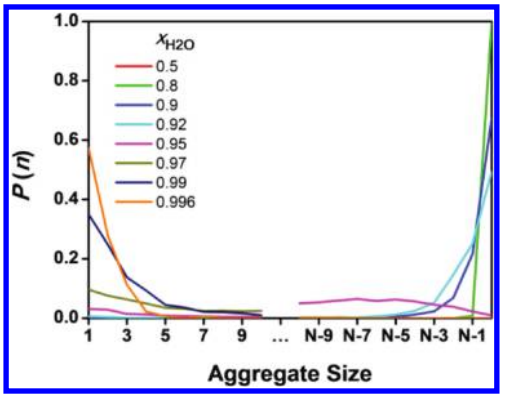

Figure 9. Size distribution of ionic liquid aggregates at different solution compositions. $P(n)$ is the probability of finding an ion (cation or anion) in an aggregate of size n; x_{H_2O} is the molar fraction of water. In the aggregate size axis, N represents the total number of ions in the simulation box (see Table 1 for details). For example, in a cluster of size N, all ions in the simulation box belong to the same aggregate.

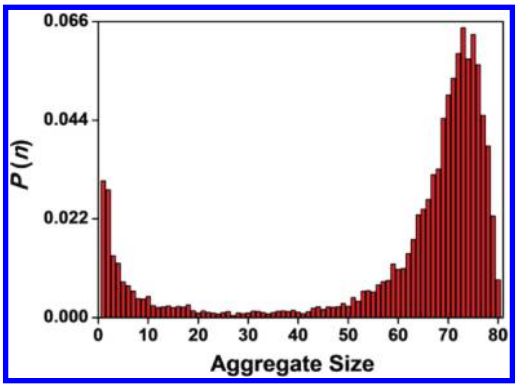

Figure 10. Size distribution of ion aggregates for $x_{H_2O} = 0.95$. $P(n)$ is the probability of finding an ion in an aggregate of size n. The existence of intermediate size aggregates indicates the proximity of the ionic liquid percolation limit.

The connectivity of the ion aggregates (number of first shell neighbors within the cluster) is analyzed in Figure 11. For solutions with $x_{H_2O} < 0.8$, the average number of neighbors of a given ion, N_{ion}, slightly decreases (from around 5 to just below 4). For higher water contents, N_{ion} rapidly drops to values below 1. This indicates, again, that below a water molar fraction of 0.8 the structure of the ionic liquid polar network is not significantly altered by the introduction of water (it loses a few connections but remains a highly branched network). It must be stressed that the large difference between the molar volumes of water and the ionic liquid (more than 1 order of magnitude) implies that $x_{H_2O} = 0.8$ corresponds, in fact, to a much lower volume fraction of water in the solution (just 0.25).[24] For concentrations in the $0.8 < x_{H_2O} < 0.95$ range, the average number of neighbors rapidly falls from ~4 to just 2, indicating significant structural modifications in the polar network. Moreover, as the water molar fraction approaches 0.95, the number of neighbors becomes approximately independent of aggregate size (Figure 11b). This suggests that in this concentration range the polar network starts to stretch, loses its branching nature, and forms chain-like structures with alternating cations and anions (each ion being connected to two counterions). However, the network remains continuous and

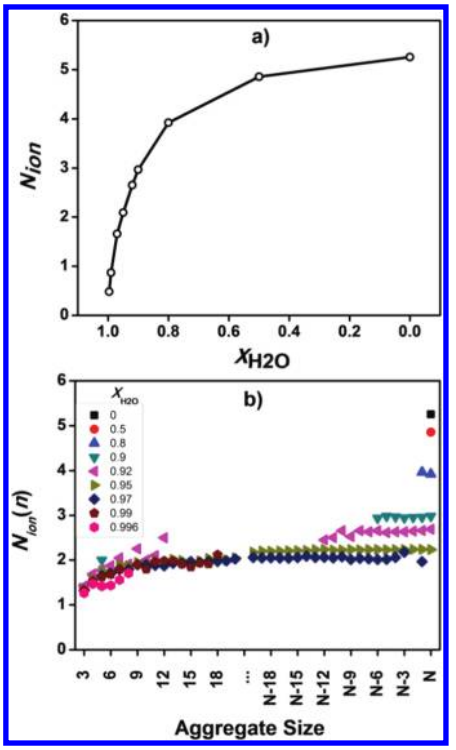

Figure 11. Number of counterion neighbors around a given ion as a function of composition. (a) Average number, N_{ion}, of neighbors for all ions (note that in this figure, for constancy with the increase of the aggregate size with x_{H_2O} decrease, the x-axis is inverted). (b) Average number of neighbors in clusters of size n, $N_{ion}(n)$.

its structure/connectivity is not significantly altered, even when a temporary detachment of a small group of ions occurs.

Around $x_{H_2O} = 0.95$, the stretching of the chain-like ionic liquid network reaches its breaking point and small ionic liquid aggregates or "icebergs"[32,33] start to form (Figure 12a and b). These become smaller as the water content increases, and for very diluted solutions, the average number of neighbors of each ion tends to zero (Figure 11a). For that reason, isolated ions are mainly observed (Figure 12c).

Solution Structure. The results presented in the previous sections suggest that the structure of $[C_2mim][EtSO_4]$ aqueous solutions changes with concentration in the following way: (i) when a few water molecules are present ($x_{H_2O} < 0.5$), they are either isolated or in small chain-like clusters; (ii) within the concentration limits $0.5 < x_{H_2O} < 0.8$, the chains grow and start to engulf the ionic liquid polar network; (iii) in the $0.8 < x_{H_2O} < 0.95$ range, after the percolation limit of water has been reached, a biphasic structure exists composed by two continuous networks; (iv) for $x_{H_2O} > 0.95$, the ionic liquid network breaks apart and only a continuous and highly branched water network remains.

It has been reported[14,15,18] that for some ionic liquids the rupture of the polar network is often accompanied by the formation of micelles. However, in the present case, no evidence of these self-organized structures has been found: instead, the results indicate the formation of chain-like aggregates before and after the ionic liquid percolation limit, which occurs for $x_{H_2O} \sim 0.95$. Furthermore, if micelles formed, the probability of finding the "tails" of the cations under close contact should increase with the progressive dilution of the solutions. However, the opposite is observed in the RDFs calculated for the distances between the

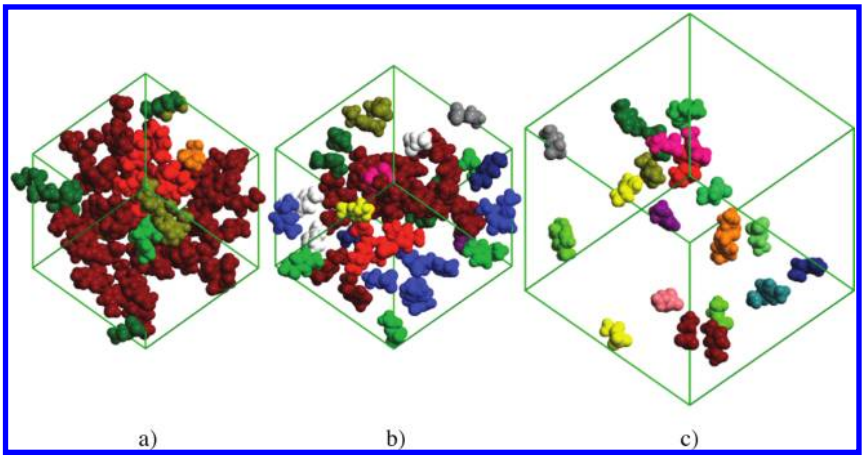

Figure 12. Snapshots of the ionic liquid aggregates in simulation boxes with (a) $x_{H_2O} = 0.95$, (b) $x_{H_2O} = 0.97$, and (c) $x_{H_2O} = 0.996$. Ions of the same color belong to the same aggregate. The pictures show that at $x_{H_2O} = 0.95$ the IL network starts to break down and multiple aggregates are formed. Finally, when just a few IL pairs are present at $x_{H_2O} = 0.996$, only isolated ions and dimers are found in solution.

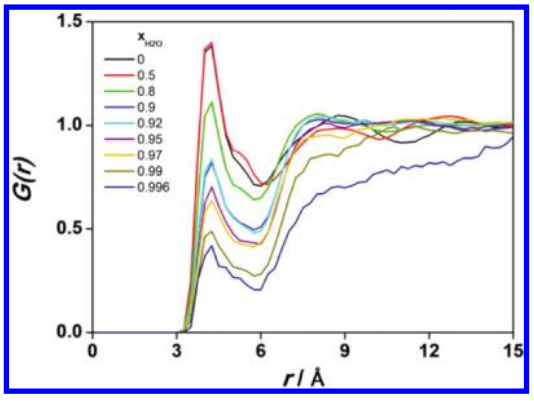

Figure 13. Radial distribution functions between the terminal carbon atoms CT of the ethyl group of the $[C_2mim]^+$ cation, showing the progressive separation of the CT atoms as the ionic liquid dilution advances.

terminal ethyl carbon atoms of the cation (Figure 13). The absence of micelles in the $[C_2mim][EtSO_4]$ aqueous solutions can be attributed to the small length of the alkyl chain (an ethyl group) in the cation. In the case of $[C_nmim][N(SO_2CF_3)_2]$ ionic liquids, for example, the formation of micelles is only observed for $n > 8$.[34]

The results in Figure 9 also show that for $x_{H_2O} > 0.9$ the probability of finding isolated ions is not negligible and increases rapidly with the water content of the solutions. For example, at $x_{H_2O} = 0.996$, the probability of finding an isolated ion is almost 60%, while the probability of finding an ion pair is only 30%. This is a somewhat unexpected result, since many ionic liquids tend to exist as dimers in diluted solutions due to the strong electrostatic interactions between cations and anions.[15,18,21] In the case of aqueous $[C_2mim][EtSO_4]$, the solvation energy of the ions by water clearly balances the loss of cation−anion interaction energy and allows the separation of $[C_2mim]^+$ from $[EtSO_4]^-$. In fact, this trend can be noticed by close inspection of the RDFs for the $O_w\cdots S$ and $O_w\cdots H2$ distances (Figure 3). As mentioned above, the first peaks of these RDFs exhibit a small shift to lower interatomic distances as x_{H_2O} increases, indicating stronger interactions between the water molecules and the ions. On the other hand, the increase of x_{H_2O} leads only to minor shifts in the first peaks of the RDFs for the $S\cdots H2$ interaction (Figure 4), an indication of less efficient interaction between the ions. This observation is also consistent with the infrared studies performed by Köddermann and co-workers,[13] which suggested that water is strongly bonded to $[C_2mim][EtSO_4]$ due to the high polarity of the latter when compared with other hydrophilic ionic liquids.

CONCLUSION

The main objectives of this work were the investigation of the structural modifications accompanying changes in concentration of $[C_2mim][EtSO_4]$ aqueous solutions and if the observed trends paralleled those previously found for the energetics of this system. Of particular interest was the analysis of the structural features corresponding to the $0.94 < x_{H_2O} < 0.99$ range, where a minimum of the enthalpy of solution of $[C_2mim][EtSO_4]$ in water had been previously found, both by calorimetric experiments and MD simulations (see Figure 6 of ref 24).

The present results have shown that two major structural events occur within this concentration range: (i) The percolation limit of the ionic liquid in water is reached; i.e., upon further dilution, the polar network of the ionic liquid (already stretched to its limit) starts to break into smaller aggregates and loses its continuous nature. (ii) The water molecules that had been growing into a second continuous network around the ionic liquid network start to experience connectivity levels among themselves similar to that of pure water (4−5 water molecules in the first neighbor shell); i.e., water starts to show properties of pure water. These two simultaneous (and interrelated) events produce significant changes in the solution energy profiles and cause the observed minimum in the trend of the enthalpy of solution values with composition. The observation that, for $x_{H_2O} = 0.996$, 60% of cations and anions are isolated indicates that at this concentration the solvation energy of $[C_2mim]^+$ and $[EtSO_4]^-$ by water clearly compensates the electrostatic interaction energy between the cation and anion, thus allowing their separation.

It must finally be stressed that the main structural features of the high dilution range are not representative of all structural modifications happening in the $[C_2mim][EtSO_4]$ solutions

throughout the full concentration range: the present work was able to identify four concentration ranges where four distinct structural regimes are present (cf. Solution Structure section): isolated water molecules ($x_{H_2O} < 0.5$); chain-like water aggregates ($0.5 < x_{H_2O} < 0.8$); bicontinuous system ($0.8 < x_{H_2O} < 0.95$); and isolated ions or small ion clusters, respectively ($x_{H_2O} > 0.95$). These include two different percolation limits: that of water in the ionic liquid network ($x_{H_2O} \sim 0.8$) and that of the ionic liquid in water ($x_{H_2O} \sim 0.95$).

AUTHOR INFORMATION

Corresponding Author

*E-mail: carlos.bernardes@ist.utl.pt (C.E.S.B.); jnlopes@ist.utl.pt (J.N.C.L.).

ACKNOWLEDGMENT

This work was supported by Fundação para a Ciência e a Tecnologia, Portugal, through Projects PTDC/QUI/66199/2006 and PTDC/QUI-QUI/101794/2008. A Post Doctoral grant from FCT is also gratefully acknowledged by C.E.S.B. (SFRH/BPD/43346/2008).

REFERENCES

(1) Wasserscheid, P.; Welton, T. *Ionic Liquids in Synthesis*, 2nd ed.; Wiley-VCH: Weinheim, Germany, 2003.

(2) Rogers, R. D.; Seddon, K. R. *Ionic Liquids IIIA: Fundamentals, Progress, Challenges, and Opportunities - Properties and Structure; Ionic Liquids IIIB: Fundamentals, Progress, Chalenges, and Opportunities - Transformations and Processes*; Americal Chemical Society: Washington, DC, 2005.

(3) Endres, F.; El Abedin, S. Z. *Phys. Chem. Chem. Phys.* **2006**, *8*, 2101–2116.

(4) Weingärtner, H. *Angew. Chem., Int. Ed.* **2008**, *47*, 654–670.

(5) Chiappe, C.; Pieraccini, D. *J. Phys. Org. Chem.* **2005**, *18*, 275–297.

(6) Keskin, S.; Kayrak-Talay, D.; Akman, U.; Hortacsu, O. *J. Supercrit. Fluids* **2007**, *43*, 150–180.

(7) Gutowski, K. E.; Broker, G. A.; Willauer, H. D.; Huddleston, J. G.; Swatloski, R. P.; Holbrey, J. D.; Rogers, R. D. *J. Am. Chem. Soc.* **2003**, *125*, 6632–6633.

(8) Han, X.; Armstrong, D. W. *Acc. Chem. Res.* **2007**, *40*, 1079–1086.

(9) Harjani, J. R.; Friscic, T.; MacGillivray, L. R.; Singer, R. D. *Dalton Trans.* **2008**, 4595–4601.

(10) Berthod, A.; Ruiz-Angel, M.; Carda-Broch, S. *J. Chromatogr., A* **2008**, *1184*, 6–18.

(11) Hanke, C. G.; Atamas, N. A.; Lynden-Bell, R. M. *Green Chem.* **2002**, *4*, 107–111.

(12) Hanke, C. G.; Lynden-Bell, R. M. *J. Phys. Chem. B* **2003**, *107*, 10873–10878.

(13) Köddermann, T.; Wertz, C.; Heintz, A.; Ludwig, R. *Angew. Chem., Int. Ed.* **2006**, *45*, 3697–3702.

(14) Jiang, W.; Wang, Y. T.; Voth, G. A. *J. Phys. Chem. B* **2007**, *111*, 4812–4818.

(15) Fazio, B.; Triolo, A.; di Marco, G. *J. Raman Spectrosc.* **2008**, *39*, 233–237.

(16) Jeon, Y.; Sung, J.; Kim, D.; Seo, C.; Cheong, H.; Ouchi, Y.; Wawa, R.; Hamaguchi, H. O. *J. Phys. Chem. B* **2008**, *112*, 923–928.

(17) Kelkar, M. S.; Shi, W.; Maginn, E. J. *Ind. Eng. Chem. Res.* **2008**, *47*, 9115–9126.

(18) Moreno, M.; Castiglione, F.; Mele, A.; Pasqui, C.; Raos, G. *J. Phys. Chem. B* **2008**, *112*, 7826–7836.

(19) Wu, B.; Liu, Y.; Zhang, Y. M.; Wang, H. P. *Chem.—Eur. J.* **2009**, *15*, 6889–6893.

(20) Danten, Y.; Cabaço, M. I.; Besnard, M. *J. Phys. Chem. A* **2009**, *113*, 2873–2889.

(21) Takamuku, T.; Kyoshoin, Y.; Shimomura, T.; Kittaka, S.; Yamaguchi, T. *J. Phys. Chem. B* **2009**, *113*, 10817–10824.

(22) Ficke, L. E.; Rodriguez, H.; Brennecke, J. F. *J. Chem. Eng. Data* **2008**, *53*, 2112–2119.

(23) del Popolo, M. G.; Mullan, C. L.; Holbrey, J. D.; Hardacre, C.; Ballone, P. *J. Am. Chem. Soc.* **2008**, *130*, 7032–7041.

(24) Leskiv, M.; Bernardes, C. E. S.; Minas da Piedade, M. E.; Canongia Lopes, J. N. *J. Phys. Chem. B* **2010**, *114*, 13179–13188.

(25) Smith, W.; Forester, T. R. *The DL_POLY Package of Molecular Simulation Routines (v.2.17)*; The Council for The Central Laboratory of Research Councils; Daresbury Laboratory: Warrington, U.K., 2006.

(26) Praprotnik, M.; Janežič, D.; Mavri, J. *J. Phys. Chem. A* **2004**, *108*, 11056–11062.

(27) Canongia Lopes, J. N.; Deschamps, J.; Pádua, A. A. H. *J. Phys. Chem. B* **2004**, *108*, 2038–2047.

(28) Canongia Lopes, J. N.; Padua, A. A. H.; Shimizu, K. *J. Phys. Chem. B* **2008**, *112*, 5039–5046.

(29) Mele, A.; Tran, C. D.; Lacerda, S. H. D. *Angew. Chem., Int. Ed.* **2003**, *42*, 4364–4366.

(30) Mele, A.; Romano, G.; Giannone, M.; Ragg, E.; Fronza, G.; Raos, G.; Marcon, V. *Angew. Chem., Int. Ed.* **2006**, *45*, 1123–1126.

(31) Kanzaki, R.; Mitsugi, T.; Fukuda, S.; Fujii, K.; Takeuchi, M.; Soejima, Y.; Takamuku, T.; Yamaguchi, T.; Umebayashi, Y.; Ishiguro, S. *J. Mol. Liq.* **2009**, *147*, 77–82.

(32) Koga, Y. *J. Phys. Chem.* **1996**, *100*, 5172–5181.

(33) Koga, Y. *J. Therm. Anal. Calorim.* **2002**, *69*, 705–716.

(34) Blesic, M.; Marques, M. H.; Plechkova, N. V.; Seddon, K. R.; Rebelo, L. P. N.; Lopes, A. *Green Chem.* **2007**, *9*, 481–490.